ARL-TN-0738 ● FEB 2016

US Army Research Laboratory

Mapping Boron Dioxide (BO_2) Light Emission During Ballistic Initiation of Boron

by Kevin L McNesby, Matthew M Biss, Richard A Benjamin, Ronnie A Thompson, and Anthony Rozanski

NOTICES

Disclaimers

The findings in this report are not to be construed as an official Department of the Army position unless so designated by other authorized documents.

Citation of manufacturer's or trade names does not constitute an official endorsement or approval of the use thereof.

Destroy this report when it is no longer needed. Do not return it to the originator.

ARL-TN-0738 ● FEB 2016

US Army Research Laboratory

Mapping Boron Dioxide (BO_2) Light Emission During Ballistic Initiation of Boron

by Kevin L McNesby, Matthew M Biss, Richard A Benjamin, and Ronnie A Thompson
Weapons and Materials Research Directorate, ARL

Anthony Rozanski
General Sciences Inc., Souderton, PA

REPORT DOCUMENTATION PAGE

Form Approved
OMB No. 0704-0188

1. REPORT DATE *(DD-MM-YYYY)*	2. REPORT TYPE	3. DATES COVERED (From - To)
February 2016	Technical Note	February 2013–February 2015

4. TITLE AND SUBTITLE
Mapping Boron Dioxide (BO_2) Light Emission During Ballistic Initiation of Boron

5a. CONTRACT NUMBER

5b. GRANT NUMBER

5c. PROGRAM ELEMENT NUMBER

6. AUTHOR(S)
Kevin L McNesby, Matthew M Biss, Richard A Benjamin, Ronnie A Thompson, and Anthony Rozanski

5d. PROJECT NUMBER

5e. TASK NUMBER

5f. WORK UNIT NUMBER

7. PERFORMING ORGANIZATION NAME(S) AND ADDRESS(ES)
US Army Research Laboratory
ATTN: RDRL-WML-C
Aberdeen Proving Ground, MD 21005-5066

8. PERFORMING ORGANIZATION REPORT NUMBER
ARL-TN-0738

9. SPONSORING/MONITORING AGENCY NAME(S) AND ADDRESS(ES)

10. SPONSOR/MONITOR'S ACRONYM(S)

11. SPONSOR/MONITOR'S REPORT NUMBER(S)

12. DISTRIBUTION/AVAILABILITY STATEMENT
Approved for public release; distribution is unlimited.

13. SUPPLEMENTARY NOTES

14. ABSTRACT
This work describes chemical imaging of boron dioxide (BO_2) formed during ballistic initiation of 1:1 by weight powder-mixtures of boron (B) and potassium nitrate (KNO_3) contained within a polyethylene spherical projectile (25-mm diameter). Initiation was achieved by impact of the gas-gun-launched B/KNO_3-filled projectile with an anvil in a windowed, air-filled chamber. To monitor the subsequent chemical reaction, a 2-camera, optically filtered method to map discrete chemical emission from the BO_2 molecule was used. This technique distinguishes incandescence of hot particles produced during the event from discrete chemical emission by BO_2 near a wavelength of 546 nm. The dependence of delay in BO_2 chemical emission (that exceeded particle incandescence) with impact velocity was investigated, and chemical emission movies, which ratio the intensity of discrete to thermal emission, are discussed. Emission spectra (300- to 1000-nm wavelength) were recorded during the impact event and used to determine a gray-body temperature of the hot particles during the time when BO_2 emission was most intense.

15. SUBJECT TERMS
boron, impact initiation, spectroscopy, ignition delay, explosions

16. SECURITY CLASSIFICATION OF:			17. LIMITATION OF ABSTRACT	18. NUMBER OF PAGES	19a. NAME OF RESPONSIBLE PERSON
a. REPORT	b. ABSTRACT	c. THIS PAGE			Kevin L McNesby
Unclassified	Unclassified	Unclassified	UU	22	19b. TELEPHONE NUMBER (Include area code) 410 306-1383

Standard Form 298 (Rev. 8/98)
Prescribed by ANSI Std. Z39.18

Contents

List of Figures

Acknowledgments

The authors would like to acknowledge the support of the US Army Research Laboratory program on Innovation Research, the Defense Threat Reduction Agency, and the Strategic Environmental Research and Development Program.

INTENTIONALLY LEFT BLANK.

1. Introduction

High-speed framing cameras have been used for decades to produce movies that help to visualize detonations and explosions.[1] While the detailed movies of these events can be qualitatively informative, retrieving variables such as pressures, temperatures, and chemical species concentrations is difficult.[2,3] Recently, some success has been realized imaging fireball surface temperatures and peak shock pressures from small- to medium-sized explosions by careful manipulation of imaging parameters.[4] These efforts enable peak pressure and temperature "maps" to be produced as the explosion proceeeds.[4] In this report, this technique is extended to mapping of chemical species arising from boron oxidation during a ballistically initiated explosion.

The overall approach used 2 synchronized high-speed cameras, filtered at different wavelengths, to map the formation of gaseous boron dioxide (BO_2) when a boron/ postassium nitrate (B/KNO_3)-filled polyethylene "bullet" is fired against an anvil in a windowed, air-filled chamber. Following impact, a ballistically initiated explosion of the B/KNO_3 powder mixture occurs. The general 2-camera method used here has been described previously.[4] To our knowledge, the work reported here is the first attempt to use the technique to map the evolution of a chemical species in an explosive event.

2. Background

Several metals and metalloids (e.g., Al [aluminum], B , Si [silicon]) may be added to propellants and explosives to increase energy.[5] For example, Eqs. 1–3 show the combustion energies (enthalpy of combustion, ΔH_c) in kilojoules per mole and kilojoules per gram of fuel for the oxidation reactions of B, Al, and Si, respectively. The combustion enthalpy of trinitrotoluene (TNT, $C_7H_6N_3O_6$, Eq. 4) is also shown for comparison.[6]

$$4B + 3O_2 \rightarrow 2B2O3_{(l)} \quad \Delta Hc = -626.8 \text{ kJ/mol} \quad \Delta Hc = -57.97 \text{ kJ/g} \quad (1)$$

$$4Al + 3O_2 \rightarrow 2Al2O3\ (l) \quad \Delta Hc = -810 \text{ kJ/mol} \quad \Delta Hc = -30.03 \text{ kJ/g} \quad (2)$$

$$Si + O_2 \rightarrow SiO2\ (\text{vitreous}) \quad \Delta Hc = -910.7 \text{ kJ/mol} \quad \Delta Hc = -32.4 \text{ kJ/g} \quad (3)$$

$$2\ C_7H_6N_3O_6 + 11O_2 \rightarrow 14CO_2 + 6H_2O + 3N_2 \quad \Delta H_c = -3410 \text{ kJ/mol} \quad \Delta H_c = -15.1 \text{ J/g.} \quad (4)$$

Because of the significant gain in combustion energy (weight basis, relative to TNT) predicted by combustion calculations, B has received considerable attention as an additive to explosive and propellant mixtures.[7] However, practical thermodynamic and physical properties inhibit realization of this ideal.[8] In a review article, Yeh and Kuo[7] summarized 2-stage B-particle combustion and measured burn times. Stepwise reactions occurring in B oxidation include[9]

$$B + O = BO. \quad (5)$$

$$BO + O = BO_2. \quad (6)$$

Equations 5 and 6 are of special interest for studies of B oxidation[10] and the work described here because excited states of the product species are responsible for the strong visible (green) light emission and offer the possibility of studying their emission as a function of ignition stimuli. Johns has shown[11] that the band structure seen in emission and fluorescence during B combustion arises from sequences of 2 electronic transitions in BO_2 gas:

$$A^2\Pi_u - X^2\Pi_g. \quad (7)$$

$$B^2\Sigma^+_u - X^2\Pi_g. \quad (8)$$

3. Experiment

3.1 B/KNO_3 Emission Spectra

Figure 1 shows the visible emission spectrum of a burning 1:1 (by weight) mixture of a military specification compliant (MIL-STD-961[12]) B/KNO_3 igniter formulation. The arrows show locations of the strongest observed emission bands of the BO_2 molecule. Off-scale features near 589 and 760 nm are emissions from sodium and potassium atoms, respectively. To obtain this spectrum, approximately 250 mg of the igniter formulation was placed on a resistively heated nickel-chromium wire ribbon. When ignited, visible light emission was measured using an Ocean Optics HR2000+ spectrograph for an integration time of 100 ms after trigger. The spectrograph was externally triggered by a Si photodiode (New Focus) coupled to a Stanford Research Systems DG535 Pulse/Delay generator.

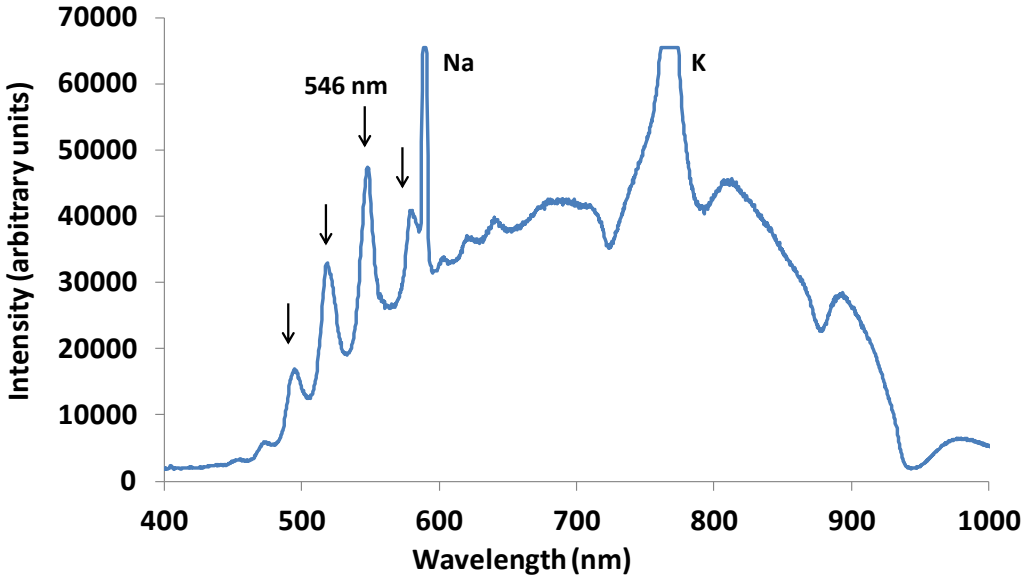

Fig. 1 Emission from a burning 1:1 (by weight) powder mixture of a milspec B/KNO_3 igniter formulation. Spectral lines from gaseous BO_2 emission (arrows) appear superimposed upon particle incandescence. Not corrected for intensity response of the spectrograph.

3.2 BO_2 Imaging

The emission spectrum of burning B/KNO_3 shown in Fig. 1 was used as a guide to devise a scheme for imaging emission from BO_2 following ballistic initiation. Early-time imaging of metal oxidation products was suggested by Dreizin for AlO emission from aluminized explosives and modified here for imaging of BO_2 emission (2012 discussion between K McNesby and EL Dreizin; unreferenced). Essentially, 2 light sensors (cameras), each filtered over a narrow wavelength region, observe an event over the same line of sight. The wavelength regions are selected so that one region coincides with a known emission band of the molecule of interest. The second region is selected so that it sees only particle incandescence (gray body emission[13]). The light signals are then ratioed to minimize the intensity from the background incandescence (subtraction gave a qualitatively similar result). For imaging BO_2 emission, the light sensors were 2 Phantom V7.3 monochrome cameras (Vision Research, Inc.) looking through a glass plate beam splitter (Edward Scientific) along a common line of sight. The cameras were run from the same time base (slave and master setup) using identical lenses, apertures, frame rate (typically 40 kHz), and exposure duration (typically 1/frame rate). For measurements of BO_2 emission, one 50-mm-diameter filter had a bandpass (10 nm) centered at 546 nm, and the other 50-mm-diameter filter had a bandpass (10 nm) centered at 700 nm. Selection of these optical regions was based upon the spectrum

shown in Fig. 1. Filters were obtained from Aurora Optical, Inc. The sensitivty of the cameras at wavelengths of 546 and 700 nm are approximately equal[13]; however, no correction was made to account for absolute differences in sensitivity.

3.3 Two-Camera Image Registration

Although an effort was made to adjust the cameras to a common line of sight, it was found that a perfectly matched, hardware-based pixel-by-pixel overlap from the 2 cameras was never actually attainable. A software program was written in the computer program MATLAB to obtain a calibration image, create a transfer matrix, and then apply this matrix pixel-by-pixel to the slave-camera images. Using this software program, a fresh camera placement and fully aligned, registered system could be achieved in approximately 10 min.

3.4 Particle Temperature Measurements

A 400-μm-diameter Si core-Si clad optical fiber (Aurora Optics, Hanover, NH) was inserted into the top of the test chamber and the distal end coupled to an Ocean Optics HR4000 visible wavelength spectrograph. As a check, light launched into this optical fiber at the spectrograph end illuminated approximately the full volume imaged by the 2-camera rig. Therefore, any light emitted during the ballistic event within the chamber would be sampled by the spectrograph. Wavelength-resolved spectra, triggered by the gas gun firing, were recorded at 15-ms intervals during the event (timing limited by the spectrograph). To measure temperature, the Ocean Optics HR-4000 spectrograph was calibrated for intensity response using an Omega Inc. Model BB-4A calibrated blackbody. Corrected intensities reported at 850 and 990 nm were used to calculate a gray-body temperature according to the Planck function.[14] This wavelength region was selected because it is free from discrete spectral emission, some spectra were saturated from 650 to 800 nm, and it was decided to use a common wavelength range for all temperature calculations. A check of the temperature measurement technique using emission from an acetylene/air diffusion flame gave reasonable results (1,800 K outer soot temperature).[15]

3.5 Light-Gas Gun

The light-gas-gun facility at General Sciences Inc. (GSI, Souderton, PA) was used to investigate the impact-velocity dependence of ignition of the B/KNO_3-filled polyethylene spheres. The gas gun consists of a high-pressure He tank, a dump valve that exhausts the high-pressure gas to the gun breech, and a 25-mm-diameter, unrifled, 4.9-m-long gun barrel. The projectile, equipped with a sabot,[16] can achieve

velocities approaching 1,200 m/s. Precise velocities are measured photonically following stripping of the sabot as the projectile exits the barrel. KNO_3 powder (50-µm particle diameter) and B powder (30-µm particle diameter) were obtained from Fisher Scientific. The hollow 25-mm-diameter polyethylene spheres were manufactured in-house at GSI.

After the velocity is measured, the spherical projectile travels 0.5 m through free space and then enters a 50-mm-diameter, burst-disk-equipped (0.18-mm thickness, Al sheet) aperture at the near end of a 2-m^3 catch tank. The far end of the cylindrical catch tank is equipped with 30-mm-thick pyrex windows that allow visualization of the projectile impact with a steel anvil at the interior wall of the tank. A schematic of the gas-gun catch-tank assembly is shown in Fig. 2, along with a color camera image (camera mounted to an optical port on top of the chamber) of an impact event using the B/KNO_3-filled polyethylene projectile.

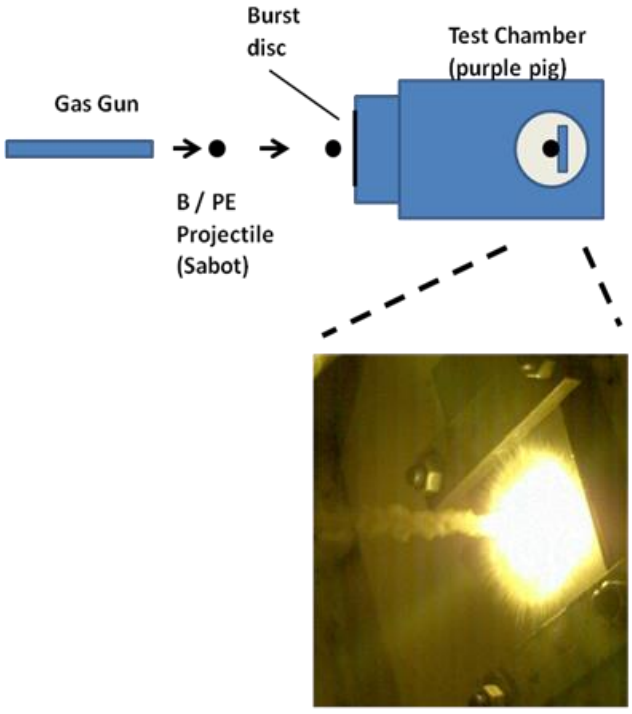

Fig. 2 A schematic of the gas gun-catch tank assembly. The photograph of the impact event is a single frame from a color camera mounted at the top of the catch tank assembly.

The field of view of the 2-camera rig was approximately 15 cm. The spherical polyethylene projectile weight was 1.25 g, the weight of the 1:1 by weight B/KNO_3 fill was 1 g (± 0.05 g), and the total projectile weight per shot was approximately 2.25 g. The 2-camera imaging rig was positioned to enable side-on imaging of the B/KNO_3-filled polyethylene sphere impacting the steel anvil at the rear interior of

the catch chamber. The focal plane of the 2-camera rig contained the projectile shot-axis. Figure 3 is a photograph of the catch chamber with the 2-camera rig in position at the experimental facility at GSI.

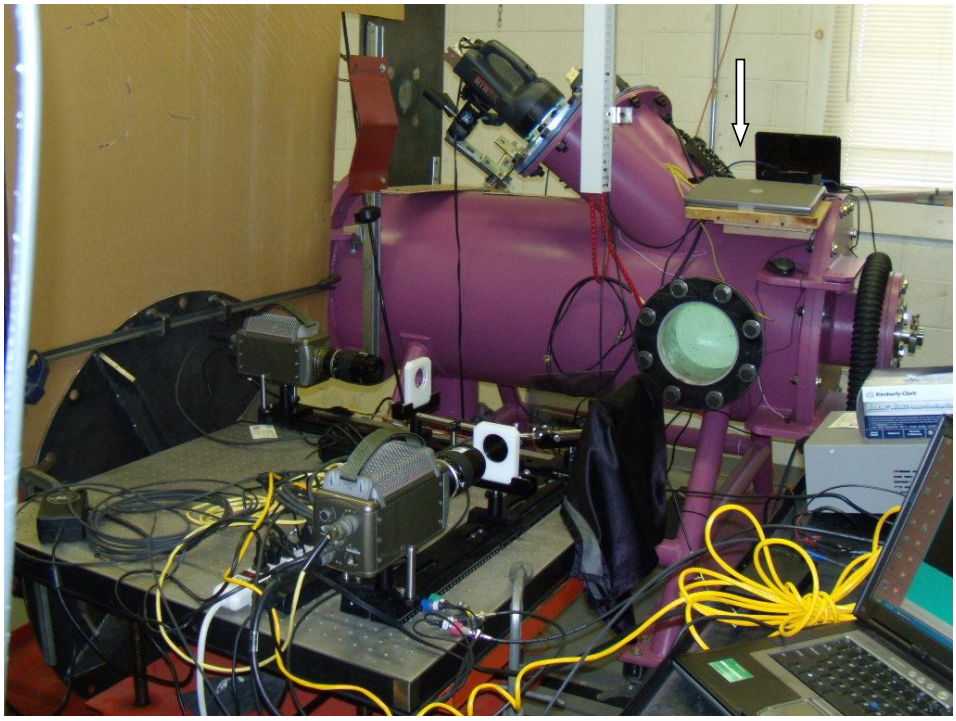

Fig. 3 The 2-camera rig in position at the side port of the catch tank, prior to a gun firing. Note the color camera at the top port of the catch tank. The gas gun is positioned to the left of the chamber, out of the field of view of the photo. An integrating spectrograph (Ocean Optics HR-4000) was mounted out of view of the photograph; however, the optical fiber that launched light from the event to the spectrograph may be seen at the top right of the catch tank (white arrow). The white plastic fixtures in front of each camera lens contain the optical filters.

4. Results

The monochrome cameras in the 2-camera rig were filtered at 546 and 700 nm (each using a 10-nm bandpass width). An examination of the emission spectrum of burning B/KNO_3 (Fig. 1) and comparison to measured spectral emission wavelengths for combusting B/KNO_3 mixtures[17] shows that the emission near 546 nm is a combination of incandescing hot particles and gas phase BO_2 emission, and the emission near 700 nm is likely due only to incandescing hot particles.

After recording a movie from each synchronized camera and registering the images as described previously, data were prepared by doing a pixel-by-pixel ratio of intensities (I_{546nm} / I_{700nm}) of each corresponding frame from each camera. If the ratio result was less than one, indicating higher intensity near 700 nm, the pixel was given a red color. If the ratio result was greater than one, indicating a higher intensity from BO_2 emission, the pixel was given a green color. Each frame-to-frame ratio produced a frame of a new movie (Fig. 4), consisting of green and red pixels only. The goal was to obtain a simple measure of how the impact velocity influenced the ratio of excited BO_2 molecules to incandescent particles.

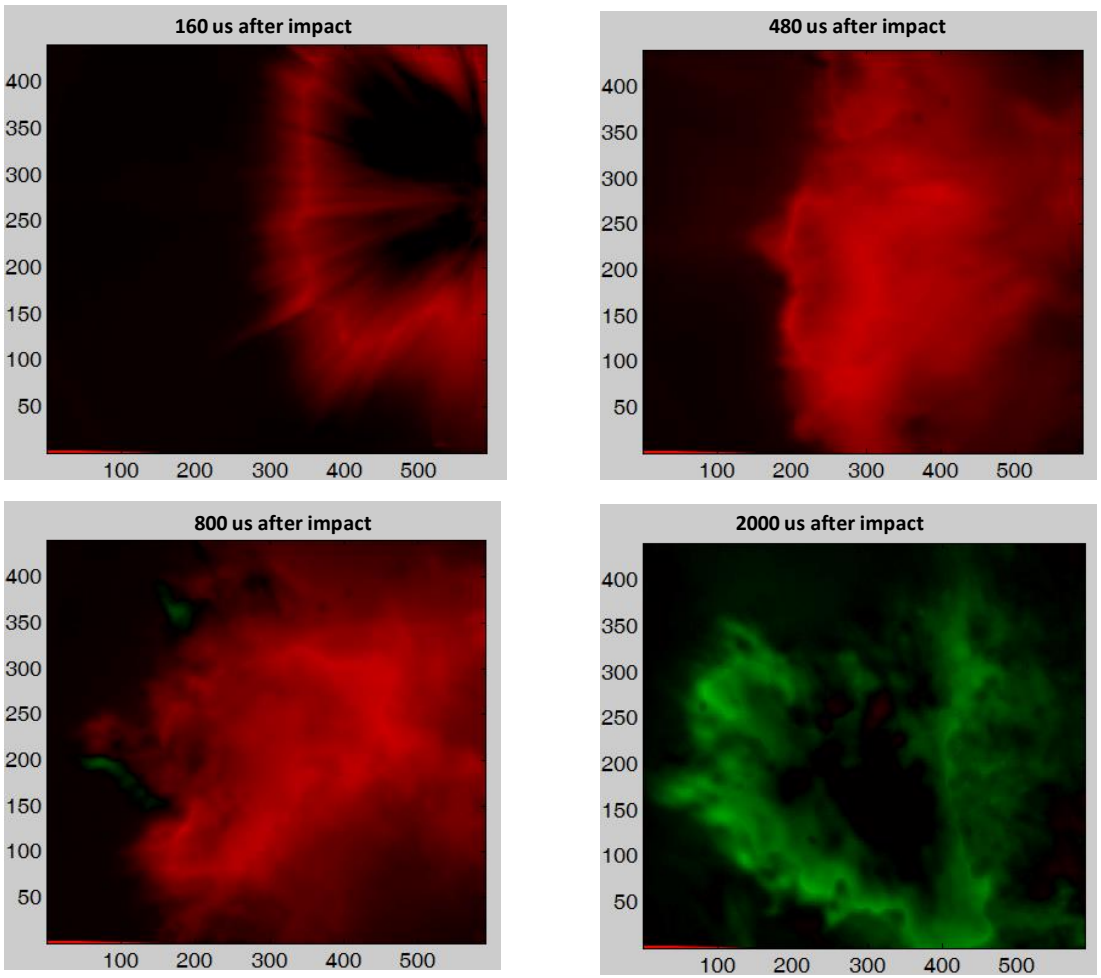

Fig. 4 A series of processed images, time after impact, that are part of an emission movie to image B oxidation/BO_2 emission. The projectile enters at the left of the figure and the anvil is at the right of the figure. Red indicates thermal emission (incandescence) near a wavelength of 700 nm and has a higher overall intensity. Green indicates emission from incandescence plus BO_2 emission near a wavelength of 546 nm and has a higher overall intensity. The x and y scales are pixel indices. Each pixel corresponds to approximately 100 μm in length at the focal plane of the 2-camera rig.

To evaluate whether impact velocity has a real influence on time to appearance of BO_2 emission using an arbitrary fixed ratio (I_{546nm} / I_{700nm} = 1), it is necessary to measure the temperature of the hot particles. Figure 5 shows a plot of average particle (incandescence) temperature (850 and 990 nm) during time of peak BO_2 emission and time to onset of BO_2 emission (I_{546nm} / I_{700nm} > 1) versus impact velocity for impact experiments of B/KNO_3-containing polyethylene spheres. Shots with polyethylene spheres that did not contain the B/KNO_3 mixture did not exhibit any of the discrete emission here attributed to B oxidation/BO_2 emission.

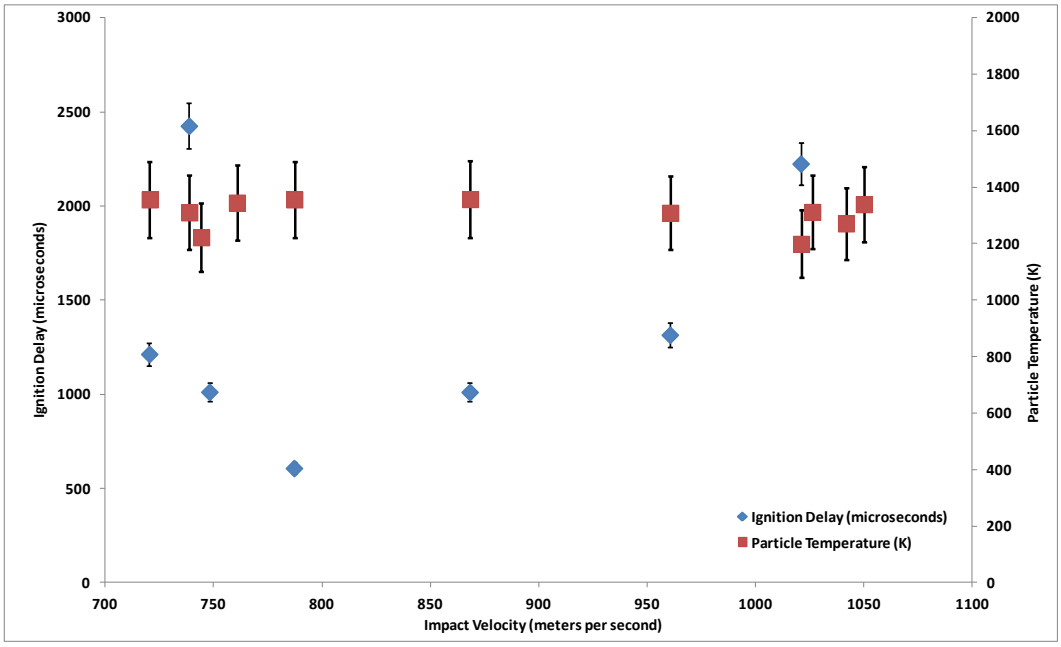

Fig. 5 A plot of particle incandescent temperature and time to onset of gaseous BO_2 emission (i.e., ignition delay) versus impact velocity for B/KNO_3-containing polyethylene spheres.

5. Discussion

Figure 5 shows that the average measured particle temperature for all experiments, during the time of most intense BO_2 emission, is near 1,400 K (± 100 K). At this average temperature the intensity of BO_2 gas emission/particle incandescence near 546 nm exceeds that of particulate emission intensity alone near 700 nm (I_{546nm} / I_{700nm} > 1). In their review, Yeh and Kuo estimate the ignition of B in air to occur at approximately 1,900 K and in oxygen at approximately 1,580 K.[7] No data are given for ignition of B/KNO_3 mixtures. The data shown in Fig. 5 suggest that onset of BO_2 emission near 546 nm in the experiment described here is dependent upon

particle temperature and has a more complicated dependence upon impact velocity. That is, once the powder mixture of B and KNO_3 reaches approximately 1,400 K, BO_2 emission becomes intense.

However, there is a shortcoming of the work presented here that should be pointed out. The camera measurements used to make the maps of BO_2 emission intensity have a temporal resolution of 20 μs. The wavelength-resolved spectral measurements, from which particle temperature is derived, have a temporal resolution of 15 ms. For each impact event, there was only one emission spectrum showing appreciable intensity, meaning the full duration of the emission event was less than 15 ms. Therefore, the temperature measurements are an average temperature during the emission event. To fully validate conclusions made in this report, it is necessary to repeat these experiments using temperature measurements at the same time resolution as the camera time resolution. If there was a brief time of high temperature (higher than the average reported here) the T^4 dependence of gray-body emission[18] intensity may still influence the average temperature. However, temperature measurements in smaller time increments than those reported here are needed to fully validate this technique.

With that caveat in mind, the data shown in Fig. 5 suggest that the imaging method described here may be of use in investigating when a metal additive participates in energy release in an energetic material formulation. The impact velocity versus onset of reaction time data shown in Fig. 5 suggests that at low velocity there is an ignition delay during which the particle is heated to approximately 1,400 K, presumably by oxidation reactions, and the ignition delay decreases as the projectile velocity increase to 800 ms^{-1}. At higher velocities, there is an apparent rise in ignition delay with impact velocity. It is conceivable that the apparent increase in ignition delay time at impact velocities above around 850 ms^{-1} may be caused by the hottest particles leaving the camera field of view as these particles are expected to have high velocities relative to particles produced at lower impact velocities. This suggests a "sweet spot", or an optimum impact velocity for minimizing time to onset of B oxidation, with these experimental parameters, for the field of view achieved with the 2-camera rig. Additionally, although it is implied that the onset of green pixels in the individual images indicates ignition delay times, the onset of green pixels actually means that the intensity of emission at 546 nm, at this time after impact, exceeds that of incandescent emission at 700 nm. For the data shown in Fig. 5, the projectile velocity at impact is believed to have an error approaching 10%, the uncertainty in time to BO_2 emission is believed to be approximately 100 μs, and the error in calculated temperature is believed to be approximately 100 K, based upon calibration measurements using emission from an acetylene/air flame.

6. Conclusion

The demonstrated chemical imaging technique may have merit, and extension to other testing scenarios may prove valuable, provided that particle temperature is always measured at similar time resolution. The ability to predetermine the time of metals participation during energy release by an explosive is not yet achievable but would be a significant accomplishment. This technique, or a refined version, may have real utility in optimizing new formulations that attempt to control the time to reaction. Additionally, as testing costs rise, the need for maximizing data per shot will mean methods similar to (or better than) those proposed here will become more important. As a practical consideration, the implementation of the software correction to register images between cameras makes the rig truly portable, with setup time approximately that for a single camera. A straightforward extension of this technique would be the incorporation of the filters into a Bayer-type chip mask, enabling a single camera rig capable of reproducing the results shown here with slightly reduced fidelity but with far simpler data manipulation.

7. References

1. Settles GS. Schlieren and shadowgraph techniques: visualizing phenomena in transparent media. Berlin (Germany): Springer-Verlag; 2001.

2. McNesby KL, Homan BE, Ritter JJ, Quine Z, Ehlers RZ. McAndrew BA. Afterburn ignition delay and shock augmentation in fuel rich solid explosives. Propellants, Explosives, Pyrotechnics. February 2010;35(1):57–65.

3. McNesby KL, Biss MM, Benjamin RA, Thompson RA. Optical measurement of peak air shock pressures following explosions propellants explosives. Pyrotechnics. 2013;35:1–6.

4. Densmore JM, Biss MM, McNesby KL, Homan BE. High speed digital color imaging pyrometry. Applied Optics. 2011;50(17):2659–2665.

5. Peuker JM, Lynch P, Krier H, Glumac N. On AlO emission spectroscopy as a diagnostic in energetic materials testing. Propellants, Explosives, Pyrotechnics. 2013;38(4):577–585.

6. Cooper PW. Explosives engineering. New York (NY): Wiley-VCH, Inc.; 1996.

7. Yeh CL, Kuo, KK. Ignition and combustion of boron particles. Prog. Energy Combust. Sci. 1996;22:511–541.

8. Miller WJ. Boron combustion product chemistry. Princeton (NJ): AeroChem Research Laboratories, Inc.; 1976 Oct. Report No.: AeroChem TP-349.

9. Brown RC, Kolb CE, Cho SY, Yetter RA, Dryer FL, Rabitz H. Kinetic model for hydrocarbon-assisted particulate born combustion. Int Journal of Chem Kinet. 1994;26:319–332.

10. Dreizin EL, Keil DG, Felder W, Vicenzi EP. Phase changes in boron ignition and combustion. Combustion and Flame. 1999;119(3):272–290.

11. Johns JWC. The absorption spectrum of BO_2. Canadian Journal of Physics. 1961;39(12):1738–1768.

12. MIL-STD-961. Department of defense standard practice for defense specifications. Falls Church (VA): Office of the Assistant Secretary of Defense (Economic Security); 1995 Mar 22.

13. Densmore JM, Biss MM, Homan BE, McNesby KL. Thermal imaging of nickel-aluminum and aluminum-polytetrafluoroethylene impact initiated combustion. Journal of Applied Physics. 2012;112:(8)084911–084911-5.

14. Herzberg G II. Infrared and raman spectra D. New York (NY): Van Nostrand Company, Inc.; 1950.

15. Sivathanu YR, Faeth GM. Temperature/soot volume fraction correlations in the fuel-rich region of buoyant turbulent diffusion flames. Combustion and Flame. 1990;81(2):150–165.

16. Burns BP, Burton L, Drysdale WH. Methodologies for forecasting sabot mass for advanced gun and projectile systems. Aberdeen Proving Ground (MD): Ballistics Research Laboratory (US); 1992. Report No.: BRL-TR-3387.

17. Snowden BS Jr. The emission spectrum of the BO_2 molecule [thesis 64-4757]. [Nashville (TN)]; Vanderbilt University; 1963.

18. Daniels F, Alberty RA. Physical chemistry. New York (NY): John Wiley and Sons; 1979.

1 (PDF) DEFENSE TECHNICAL INFORMATION CTR DTIC OCA

2 (PDF) DIRECTOR US ARMY RESEARCH LAB RDRL CIO LL IMAL HRA MAIL & RECORDS MGMT

1 (PDF) GOVT PRINTG OFC A MALHOTRA

3 (HC) US ARMY RSRCH OFC RDRL ROE V R HARMON AMSRD ARL RO P R ANTHENIEN J PARKER PO BOX 12211 RSRCH TRIANGLE PARK NC 27709

1 (HC) DARPA/DSO J GOLDWASSER 3701 FAIRFAX DR ARLINGTON VA 22203-1714

2 (HC) US ARMY AMRDEC AMSRD AMR PS PT J NEIDERT P JOHNS BLDG 7120 REDSTONE ARSENAL AL 35898

1 (HC) US ARMY ARDEC AMSRD AAR AEE W R DAMAVARAPU BLDG 2028 PICATINNY ARSENAL NJ 07806-5000

4 (HC) US ARMY ARDEC AMSRD AAR AEE W R SURAPANENI E BAKER AMSRD AAR MEE W S NICOLICH A DANIELS BLDG 3022 PICATINNY ARSENAL NJ 07806-5000

3 (HC) US ARMY ARDEC AMSRD AAR AEE W E CARAVACA RDAR MEE W J O'REILLY W BALAS-HUMMERS BLDG 382 PICATINNY ARSENAL NJ 07806-5000

1 (HC) US ARMY ARDEC RDAR MEF E D CARLUCCI BLDG 94 PICATINNY ARSENAL NJ 07806-5000

1 (HC) US ARMY PEO AMMO SFAE AMO CAS P MANZ BLDG 172 PICATINNY ARSENAL NJ 07806-5000

1 (HC) US ARMY PEO AMMO V MATRISCIANO BLDG 171 PICATINNY ARSENAL NJ 07806-5000

1 (HC) NAVAL RSRCH LAB TECH LIB WASHINGTON DC 20375-5000

1 (HC) OFC OF NAVAL RSRCH C BEDFORD 875 N RANDOLPH ST RM 653 ARLINGTON VA 22203-1927

2 (HC) NAVAL AIR WARFARE CTR CODE 470000D A ATWOOD S BLASHILL 2400 E PILOT PLANT RD STOP 5001 CH1NA LAKE CA 93555-6107

2 (HC) DTRA S PEIRIS B WILSON 8725 JOHN J KINGMAN RD MS 6201 FORT BELVOIR VA 22060-6201

30 DIR USARL
(26 PDF RDRL WM
3 HC P BAKER
1 CD) B FORCH
RDRL WML
M ZOLTOSKI
RDRL WML A
F DE LUCIA
W OBERLE
RDRL WML B
J GOTTFRIED
J CIEZAK-JENKINS (3 HC, 1 CD)
J MORRIS
B RICE
W MATTSON
R PESCE-RODRIGUEZ
B HOMAN
R SAUSA
N TRIVEDI
I BATYREV
RDRL WML C
B ROOS
K MCNESBY
E BUKOWSKI
S AUBERT
RDRL WML D
R BEYER
RDRL WML E
P WEINACHT
RDRL WML F
D LYON
RDRL WML G
T BROWN
RDRL WML H
J NEWILL
RDRL WMM
J ZABINSKI
RDRL WMP
T BJERKE